ISSN: 0976-9102(ONLINE)
DOI: 10.21917/ijivp.2014.0107

UNSUPERVISED WOUND IMAGE SEGMENTATION

K. Sundeep Kumar[1], C. F. Jacob[2] and B. Eswara Reddy[3]

[1]*Department of Information Science and Engineering, SEA College of Engineering & Technology, India*
E-mail: sundeepkk@yahoo.co.in

[2]*Department of Computer Science and Engineering, CMR Institute of Technology, India*
E-mail: cfjacob026@gmail.com

[3]*Department of Computer Science and Engineering, JNTU College of Engineering, India*
E-mail: eswarcsejntu@gmail.com

Abstract

The purpose of our research is to introduce two unique approaches for the unsupervised segmentation of wound images. The first method of segmentation is by using the texture of the image and is performed using the multi-channel filtering hypothesis for the processing of visual or optical data during the preliminary stages of the Human Visual System. We obtain the different channels from an image by filtering the image using a Gabor Filter Bank. The textural features are obtained from each filtered image and the final segmented image is acquired by reconstructing the original input image from these filtered images. The second method of segmentation was performed using parametric kernel graph cuts. Using a kernel function we transform the image data implicitly such that a piecewise constant model of the graph cut interpretation is now applicable. The objective function comprises of an original data term in order to assess the deviance of the transformed data from the initial input data within each partition. This method avoids sophisticated modelling of the input image data while availing of the computational advantages of graph cuts. By using a conventional kernel function, the energy minimization boils down to image partitioning via graph cut iterations and assessments of region parameters by means of fixed point calculations. The efficacy and flexibility of both the methods are established by carrying out investigations on real wound images.

Keywords:

Gabor Filter Banks, Graph Cuts, Radial Basis Function (RBF), Wound Healing, Human Visual System (HVS)

1. INTRODUCTION

Image segmentation is a challenging and essential task in the fields of computer vision and image processing. The intention of image segmentation is to divide the wound image into separate regions based on various characteristics and parameters. Taking into consideration the wound images two approaches have been taken to segment them. Firstly, based on the variance in the spatial arrangement of the pixels the wound image can be partitioned using the textural cues and is referred to as textural segmentation. The textural segmentation is carried out by filtering the image using a Gabor Filter Bank [18] - [21] and then reconstructing the final image using the input image as the basis. The other method of segmentation is by modelling the input image as a graph and then partition the image into regions by considering the pixels as nodes [27] - [31]. Before going into a deep explanation on how these methods were employed a brief introduction of the various stages of wound healing and the different types of tissues that are to be segmented is required. Consequently, the following paragraphs give us an overall look at the stages and tissues involved in wound healing.

In essence the capability of an organism to repair or fix itself is called Wound Healing. This activity is either visible (noticeable) such as a cut becoming smaller in size or microscopic (not noticeable) for instance fresh cells taking the place of damaged cells, both transpire on a day-to-day basis and together they are characterized by the term Regeneration (which means renewal or restoration or reinforcement). Good examples of regeneration with respect to the animal kingdom are lizards that restore their lost tails, the starfish that can grow a new tentacles in place of severed ones, crabs that replace claws and earthworms can substitute a majority of its body. Of course these examples are rather far-reaching when compared to the human body as we do not have the capacity to replace any of our severed limbs. Hence it is paramount that wounds are diagnosed and treated before limbs, organs or even lives are lost.

There are three phases of wound healing [1], [2], [3], [4] and [5] i.e. the inflammatory, proliferative or fibroblastic, and maturation or remodelling stages. In case of a cut or laceration, the wound healing process commences with inflammation and the biochemical constituents gather as the wound site swells. Some of the biochemical ingredients are prostaglandins, leukocytes and monocytes fibrinogen, histamine and vasoactive substances. This phase contains a lot of activities which must come to pass to get the wound ready for the subsequent stages of wound healing. Non-steroidal anti-inflammatories (NSAIDs) are used for the treatment of inflammation and pain but, they actually limit inflammation. These NSAIDs are common drugs prescribed by doctors for patients of any age. The next stage involves the proliferation of fibroblasts as they situate themselves for collagen synthesis and the wound site is strengthened as the collagen content increases. The maturation or remodelling phase is the concluding phase of the wound healing process and lasts the longest. This phase could carry on for weeks or even numerous years (based on the severity of the wound), with gradual enhancements in the wound's appearance. Surgical procedures (treatments) or operations may possibly hamper the harmonious balance of the human body and will take time for the body to adjust. Slow and steady wound healing must be supported under these circumstances; Fig.1, shows the different stages of wound healing.

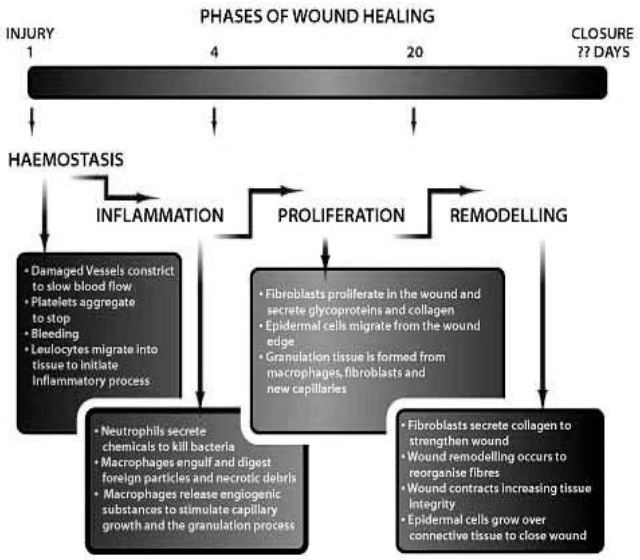

Fig.1. Stages of wound healing

A brief explanation on the types of tissues and how they are formed provides a better understanding as to how the wound image segmentation helps in diagnosis and treatment of various wounds as explained in [1] - [5]. The rudimentary tissue is called the Granulation tissue that emerges during the inflammatory phase, which lasts for a period of two to five days after the lacerating and cedes its growth once the wound bed is sealed off. The lifeless or dead tissue is called the Necrotic tissue and is the consequence of inadequate blood supply to the site of the wound. The fragmentation of dying cells generates debris and dead cells, which are the premier components of the Necrotic tissue. As the Necrotic tissue becomes more dehydrated it shifts colour from red to brown or black/purple. Ultimately, it develops a thick black leathery dry structure called eschar. The formation of the Necrotic tissue can be perceived in a vast array of wound types, including various chronic wounds and burns. In stark contrast, Slough is a yellow fibrinous tissue that comprises of pus, proteinaceous material and fibrin. Slough is understood to be linked to bacterial activity and can be located on the surface of a formerly clean wound bed. Wound healing is hampered by the build-up of necrotic tissue or slough as they promote bacterial colonization and is of great clinical significance. Clearly a method of delineating boundaries from a wound image would be of great importance as both diagnosis and treatment can be greatly improved. The other point to be noted is that images acquired are of very high quality and hence providing a very high level of detail.

In [6] the Support Vector Machine has been used to classify the data. The training data used in this method has been segmented using either supervised or semi-supervised methods. In the proposed method we have used two unsupervised methods to segment the data. The main advantage of using unsupervised methods is to eliminate human errors. The other technique that can be used for the wound image segmentation is colour image processing. Methods such as Statistical Region Merging [24], JSEG [25] and Colour Structure Codes [26] have been proposed in the past. The main drawbacks of these methods are that they over segment the image. In doing so, valuable information may be lost. The other weakness of colour image segmentation is that colour quantization is used while processing the image as it reduces the time. When quantization of the image is carried out regions that are separate but, have a similar colours will be grouped into a single region. This is not a good practice especially when colour is the main feature that is to be used in processing the image.

The Gabor Filter Bank method proposed by [18] is used first for unsupervised segmentation. It is said to be the closest explanation on how the visual system works in mammals [23]. It has been proved by [23] that the Human Visual System (HVS) breaks down the images acquired by the eyes into a number of filtered sub-signals. These signals can be interpreted as one dimensional and two dimensional images when they are merged. Hence by using this method we can segment the image based on its texture in a completely unsupervised manner using different frequencies and orientations which will be explained in detail in the latter part of this paper.

The other method we have proposed is using Parametric Kernel Graph Cuts [28]. This method involves the use of a kernel function to separate the data. The kernel being used here is an RBF kernel. The reason for using an RBF kernel is because it works seamlessly with graph cuts and is predominantly used for data clustering, which is nothing but partitioning as is our case. The Radial Basis Function (RBF) is used to distinguish between different sets of values based on certain features. Compared to the original Graph Cut method proposed in [27], we see there is a significant improvement in the final segmentation of the image.

Section 2, 3, 4 and 5 explain the methods used in detail. Section 6 illustrates the results followed by the section 7 that contains the conclusion.

2. GABOR FILTERS

The immense assortment of artificial and natural textures makes sure that a universal definition of texture is out of the question. The multi-channel filtering theory proposed by Campbell and Robson [23], maintains that the Human Visual System (HVS) breaks down the retinal image into numerous filtered images, each one of these images contain intensity deviations over a constricted scope of orientations and frequencies. Each texture has unique dominant spatial-frequency constituents and for this reason the multi-channel filtering approach produces good results. The biggest benefit of the multi-channel filtering approach lies in its simplicity as the grey-level image is filtered or decomposed into many filtered images using basic statistics with a limited amount of spectral information. The main concerns with the multi-channel filtering approach to texture analysis are: 1) Figuring out the number of channels and the functional characterization of the same, 2) Feature extraction (texture features) from the filtered images, 3) The bond between channels (independent vs. dependent) and 4) The discrete channels are integrated to yield a segmentation.

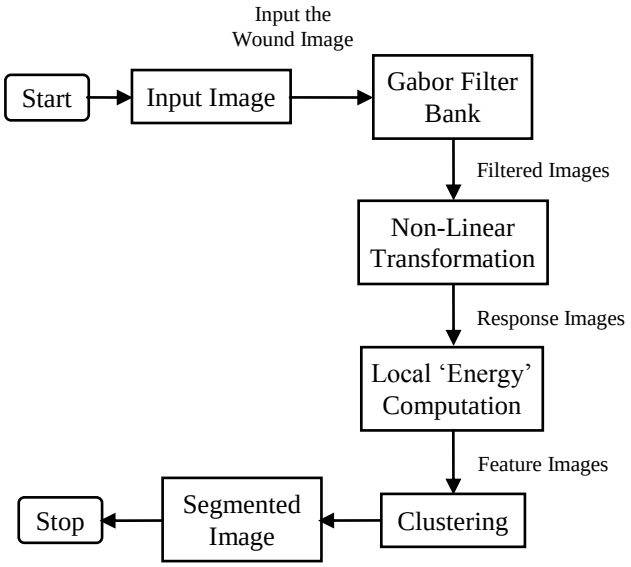

Fig.2. An overview of the texture segmentation algorithm

In this method the spatial arrangement of the values of the adjacent pixels is used for the purpose of image segmentation. This can also be described as the differences in texture of the image. A multi-channel filtering [18] approach has been used in our work. The segmentation of images is done by reconstruction of the original wound image from the group of filtered images using a set of filters called the Gabor Filter Bank and these filters will be selected in a systematic manner. The functional characterization of the channels is done by using the Gabor Filter Bank. Using the Gabor function as the wavelet, the set of filters comprising the Gabor Filter Bank must form an approximate basis for the aforementioned wavelet transform. Each one of the filtered images undergoes a constrained non-linear transformation that works as a 'blob detector'. Multi-scale blob detection is implemented by combining the non-linear transformations and the multi-channel filtering stages. The texture discrimination is performed by identifying the blobs in different regions which have differences in the attributes. The characteristics of the blobs are acquired by the texture features that are described by the evaluation of 'energy' within a small window surrounding each pixel in each response image using a statistical approach. In doing so, this process produces a single 'feature image' that corresponds to the related filtered image as shown in Fig.2. The window size varies for each response image and is established based on the radial frequency of the corresponding filter. The texture segmentation system involves the following steps:

- Decomposition of the input image using a filter bank
- Computing Feature Images (Feature extraction)
- Dependent vs. Independent channels
- Clustering

2.1 FILTER BANK

The channels are characterized by the two-dimensional Gabor Filter Bank. The two-dimensional Gabor function is a two-dimensional Gaussian that is modulated with respect to both frequency and orientation. In the spatial domain the Gabor filter is represented by,

$$g_{\lambda\theta\psi\sigma\gamma}(x,y) = \exp\left(-\frac{x'^2+\gamma^2 y'^2}{2\sigma^2}\right)\cos\left(2\pi\frac{x'}{\lambda}+\psi\right) \quad (1)$$

where,

$$x' = x\cos(\theta) + y\sin(\theta) \text{ and } y' = y\cos(\theta) - x\sin(\theta).$$

In this equation, λ represents the wavelength of the cosine factor, θ represents the orientation of the normal to the parallel stripes of a Gabor function in degrees, ψ is the phase offset in degrees, γ and is the spatial aspect ratio and specifies the elliptically of the support of the Gabor function, and σ is the standard deviation of the Gaussian determines the (linear) size of the receptive field. The Fig.3 below shows an example of a two-dimensional Gabor Filter.

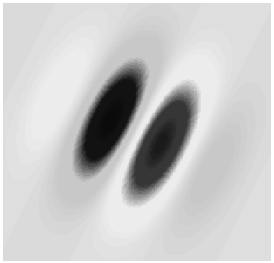

Fig.3. Example of a 2D Gabor Filter

Both the spatial-frequency and the spatial domains have to be measured concurrently in order to ensure Texture Segmentation. There must be a trade-off between filters localized in the spatial domain that offer precise localization of texture edges and filters localized to the spatial-frequency domain have smaller bandwidths and make finer distinctions between the various textures. On the other hand, the bandwidth of a filter in the spatial-frequency domain is inversely related its effective width in the spatial domain. Gabor filters provide us with a favourable solution as they exhibit optimal joint localization with respect to both the spatial-frequency and the spatial domains. In our implementation, we use a 'fixed' set of Gabor filters to model the various channels and also as an added bonus they preserve most of the information offered by the input image.

2.2 CHOICE OF FILTER PARAMETERS

We use orientation separation angles of 30° as recommended in [19], that is:

θ: 0^o, 30^o, 60^o, 90^o, 120^o, 150^o

Psychophysical experiments show that the resolution of the orientation tuning ability of the HVS is as high as 5°. Therefore, in general, smaller orientation separation angles will be necessary. The restriction to six orientations is made for computational efficiency. The following values of frequencies were used as recommended in [20].

$$f_1 = 0.25 - 2^{i-0.5}/I$$

$$f_h = 0.25 + 2^{i-0.5}/I$$

where, i = 1, 2 ... log2(I/8), I is the width of image which is a power of 2. Note that $0 < f_{1(i)} < 0.25$ and $0.25 \le f_{h(i)} < 0.5$. For

an image with 256* columns, for example, a total of 60 filters can be used in 6 orientations and (5 + 5) frequencies. In this paper we set the value of the bandwidth b of the Gabor filter to 1 octave as in [18].

On closer inspection we see that the wavelet transformation is quite similar to the Window Fourier Transform. Conversely, the window size with respect to each transformation behaves in a contrasting manner as it adjusts itself corresponding to the frequency in a wavelet transform but remains fixed in window Fourier transforms. As explained in [21] the wavelet transform is used as a band-pass filter on the input wound image. The advantage of the Gabor function is that it can be used the basis for the wavelet transform as explained earlier and in addition the non-linear transformation of the wound image does not give rise to orthogonal decomposition. The studies of [21] also show that unlike textures produce responses of different intensities, which is essential in texture analysis while using the multi-channel methodology. The filters exploit the dissimilarities in both orientation and size (spatial-frequency) as the decomposition achieved by the Gabor Filter Bank or Set is almost orthogonal, and this is because in the spatial-frequency domain the filters hardly overlap.

2.3 COMPUTING FEATURE IMAGES (FEATURE EXTRACTION)

Jain [18] recommended the nonlinear sigmoid function provides a good output

$$\tanh(\alpha t) = \frac{1 - e^{-2\alpha t}}{1 + e^{-2\alpha t}} \tag{2}$$

where, α is a constant. The nonlinear sigmoid function also saturates the output of the filters and is very similar to the activation function used in artificial neural networks. Using Eq.(2) the sinusoidal modulations are transformed into square modulations on filtering the image and hence it behaves as a blob detector. Since Eq.(2) is odd symmetric, the blobs detected are multiple in nature it is far more simple and efficient to take the mean of the small overlapping windows and use it to calculate the average absolute deviation (AAD), instead of detecting separate blobs.

When smaller windows are used the boundaries of the regions are well defined, conversely larger windows provide a more precise measurement of the texture features. To get a more accurate localization of the boundaries of each texture region, Gaussian weighted windows are used. The Gaussian window used to filter each image whose space constant σ varies proportionally to the average size of the variations in the intensities of the image. Considering, a Gabor filter the average size with radial frequency u_0 is represented by,

$$T = N_c / u_0 \text{ pixels},$$

where, N_c, is the number of columns (width) of the image. We use the Gaussian smoothing function to remove any noise that may be present in the image. It is given by,

$$g(x, y) = \exp\left(-\frac{x^2 + y^2}{2\sigma^2} \right) \tag{3}$$

where, σ is the standard deviation which determines the (linear) size of the receptive field (window size).

2.4 CLUSTERING

K-means is one of the simplest and most commonly used unsupervised learning algorithms used for the purpose of clustering. The numbers of clusters is fixed a priori and have '*k* centroids', to represent each cluster. The best option is to place the centroids as far away from each other as possible. At the next stage the centroid is linked to the given dataset via the value closest to it and once all the values (points) are linked an early grouping of the data is obtained. The centroids have to be revaluated as the values are associated to the centroids in a very crude manner and the revaluation of the centroids are preformed repetitively until the centroids' positions do not change anymore. The fundamental principle of the K-means algorithm is to minimize the *objective function*, in our case it is to minimize the squared error and it is given by,

$$J = \sum_{j=1}^{k} \sum_{i=1}^{n} \left\| x_i^{(j)} - c_j \right\|^2$$

where, $\left\| x_i^{(j)} - c_j \right\|$ is a chosen distance measure between the cluster centre c_j and a data point $x_i^{(j)}$. It explains the distance between the *k* centroids and the *n* data points of the dataset. In a simple manner the standard K-means algorithm to cluster the texture regions is explained in the following steps

Step 1: Initialize centroids of K-clusters randomly.

Step 2: Assign each sample to the nearest centroid.

Step 3: Calculate centroids (means) of K-clusters.

Step 4: If centroids are unchanged, done. Otherwise, go to Step 2.

Additionally, the spatial adjacency information is obtained from the spatial coordinates of the pixels to further enhance the clustering process and was first proposed by [18].

3. GRAPH CUTS

Typically the piecewise model or its Gaussian generalization is used in graph cut methods that do not need user inputs and this is because we can denote the data term in the form desired by the standard graph cut algorithm [27], [33], [35], [36]. Then again, these models are not applicable for the segmentation of wound images. In wound images, different regions demand for different models. With respect to sonar imagery the Gaussian distribution is used to model the shadow regions precisely and the reverberation regions are modelled by the Rayleigh distribution accurately as proven in [47]. Taking this example into consideration we can conclude that the parameters of subjective models are not governed by the data in a manner that would safeguard the kind of data term needed by the standard graph cut algorithm and hence these types of models cannot be used. However, owing to the way in which linear patterns of the image data can be attained from the discrete approximation of the Gaussian parameters the same can be used as the objective function. Also, the objective function has to be influenced by the

sum over all pixels of the pixel itself and the pixel neighbourhood dependent data as well as the variables. The graph cut algorithm also requires all variables that are global with regard to all the partitioned regions, be inapplicable if they cannot preserve the intended form of the data term.

One approach of introducing a universal model is to involve user interaction. The interactive graph cut methods can be implemented in a generic manner by adding a procedure that learns the region parameters at every stage of the graph cut segmentation to the Gaussian process. Though these parameters supplement the data at each phase the region parameter learning and the graph cut segmentation procedure are loosely coupled meaning that they are not a consequence of optimizing the objective function. In most cases interactive methods segment the images into the foreground or background regions i.e. two regions. Research studies in [29] - [32] have used mixtures of Gaussians and have defined the regions using their image histograms. Interactive methods cannot be used for multiregion segmentation as general models like mixtures of Gaussian and histograms turn out to be intractable. Keep in mind by learning the specific model in advance, the given model can be used in the unsupervised graph cut segmentation. Now, the model turns into a portion of the data. But, as explained in [48] this type of modelling is both time consuming and extremely difficult. Furthermore, a model learned using examples from a set of images in not applicable for all of the images especially those from a different class.

The multiregion wound image segmentation must provide a more general model than the Gaussian and hence kernel mapping was chosen as a method that could be used for the unsupervised graph cut formulation. The non-linear image data is implicitly mapped into data points of a higher dimensional space using a kernel function which allows for the formulation of the unsupervised graph cut and piecewise constant model becoming applicable as illustrated in Fig.4. From [38] we can concur that the mapping is implicit as the dot product and hence the Euclidean Norm of the transformed data in a higher dimensional space can be articulated using the kernel function without explicitly calculating the transform. The studies [38], [39], [40], [49], [50], [51], [52] have presented proof that complex structured data can be clustered properly by established kernels that are used in pattern classification. The studies conducted in [53] prove that kernel mapping ought to be relatively effective with respect to the segmentation of all sorts of images, because it provides the interpretation of image segmentation as the clustering of image data with spatial constraints.

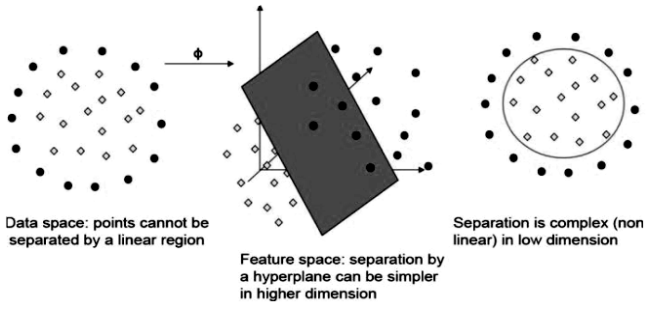

Fig.4. Illustration of the separation of non- linear data by mapping the data to a higher dimensional space

The proposed functional has two terms: a regularization term put across as a function of the indices of the region and an initial kernel-induced term that calculates the deviance of the image data inside each region when compared to the piecewise constant model. Utilizing a popular kernel function, the minimization of the objective function is done by iterating two consecutive steps: 1) minimization by graph cuts with regard to the wound image segmentation and 2) minimization using fixed point computation with regard to the regions parameters. The proposed method benefits from both optimization of the graph cut method as well as the simplicity in modelling of the wound image data. The proposed method has a higher accuracy and exhibits better flexibility when compared to the present methods of wound image segmentation. Section 4 re-examines the graph cut image segmentation generally identified as a maximum a posteriori (MAP) approximation problem in [29], [30], [31], [36]. The graph cut segmentation functional's kernel-induced data term is presented in section 5 along with the functional optimization equations and the ensuing algorithm.

4. WOUND IMAGE SEGMENTATION USING UNSUPERVISED PARAMETRIC GRAPH CUTS

Considering $I : p \in \Omega \subset \mathbb{R}^2 \rightarrow I_p = I(p) \in X$ as the image function from a positional array Ω to a space X of variables such as colour, intensity, pixel relationships, texture vectors and spatial location of pixels. Segmenting the image I into N partitions in the discrete image domain involves of finding a partition $\{R_l\}_{l-1}^{N}$ so as to ensure that each region is constant with regard to the characteristics of the wound image.

The image segmentation process is modelled as a label assignment problem by graph cut methods. Segmentation in the image domain Ω is carried out by allotting a label l from a limited set of labels L. A region R_l is characterized by $R_l = \{p \in \Omega | p$ is labelled $l\}$ and a set of pixels labelled by l. The problem involves minimizing the given functional depicting a set of constraints by prudent labelling of pixels. From [29], we concur that the functionals that are most commonly used, especially in several challenges faced by computer vision are the sum of two distinctive terms: a regularization term (the prior) for the boundaries of the smooth regions and a data term to assess the compliance of the wound image data encompassed by the segregated regions to a statistical model. From [29], [30], [31], [32], [35], [36], [37], [42], [43], [44] we see that various current methods portray wound image segmentation as a MAP estimation problem, assuming the model distributions inside regions $P(I_p/R_l)$ the optimization of the region term is done by maximizing the conditional probability of pixel data. With regards to interactive image segmentation, these model distributions are obtained from user interactions [30], [31], [32]. Keeping this in mind, Mixture of Gaussians Models (MGM) [31] and Histograms [30] are generally used for the purpose of estimating model distributions. From the perspective of unsupervised image segmentation certain parametric distributions (for example the Gaussian model), were receptive to the method of graph cut optimization [36], [37]. Let λ be the indexing function where λ allots every single point of the wound image to one of the regions, now the segmentational functional is given by

$$\lambda : p \in \Omega \rightarrow \lambda(p) \in L \tag{4}$$

where, L is the finite set of labels, with cardinality less than or equal to N. Using Eq.(4) the segmentational functional can be represented by,

$$F(\lambda) = D(\lambda) + \alpha R(\lambda) \tag{5}$$

where, D is the data term, α is the positive factor and R is the prior. The MAP formulation using the given parametric model and Eq.(5) expresses the data term as,

$$D(\lambda) = \sum_{p \in \Omega} D(\lambda(p)) = \sum_{l \in L} \sum_{p \in R} -\log P(I_p / R_l) \tag{6}$$

Recently numerous studies [33], [36], [37] have fixated on the piecewise constant segmentation model, a specific case of the Gaussian distribution since the forthcoming algorithms are computationally simple. The piecewise constant model parameter μ_l of partition R_l modifies the data term and now it is given by,

$$D(\lambda) = \sum_{p \in \Omega} D_p(\lambda(p)) = \sum_{l=L} \sum_{p \in R_l} (\mu_l - I_p)^2 \tag{7}$$

The prior is now,

$$D(\lambda) = \sum_{p \in \Omega} D_p(\lambda(p)) = \sum_{l \in L} \sum_{p \in R_l} (\mu_l - I_p)^2 \tag{8}$$

with N a neighbourhood set consisting of all the neighbouring pairs of pixels and $r(\lambda(p), \lambda(q))$ is the smoothness regularization function obtained from the truncated squared absolute difference [33], [34], [36]. Consider const is a constant then we get,

$$r(\lambda(p), \lambda(q)) = \min\left(const^2, \left| \mu_{\lambda(p)} - \mu_{\lambda(q)} \right|^2 \right). \tag{9}$$

As explained in the previous section the piecewise constant model is not usually applicable even though it is the most frequently used. In the ensuing section, a data term which allusions the transformed wound image data using a kernel function is introduced and the advantages and intention behind doing so are explained in detail.

5. SEGMENTATION FUNCTIONAL FOR THE WOUND IMAGE IN THE KERNEL INDUCED SPACE

Since the wound image data is fairly complex, computationally efficient models like the piecewise Gaussian distribution are insufficient in partitioning the linearly inseparable data. In this method, kernel functions are employed for the image data transformation. Instead of coming up with complex image models that are very precise in order to address the non-linear problem, the data is implicitly transformed using a mapping function ϕ which is nonlinear by nature. In doing so the piecewise constant model is now capable of partitioning the data in the mapped domain as though it was linear (refer to Fig.4). The most important part to remember while using this method is that there no longer exists a need to explicitly calculate the mapping of ϕ. Using Mercer's Theorem [38], the scalar product in the feature space is enough to define the data term induced by the kernel as a function of the wound image, the kernel function and the partitions parameters. The main advantages of this method are that neither user interaction nor prior knowledge is required.

5.1 FUNCTIONAL

Considering $\phi(.)$ as a non-linear mapping from the observational domain of lower dimensions X to a higher (perhaps infinite) dimensional mapped/feature domain $\Im$. A prearranged labelling allocates every single pixel a label (weight) and hence the image space is split into different regions. A single label is used to describe each region and is mathematically shown as $R_l = \{p \in \Omega | p = l\}$, $1 \leq 1 \leq N$. Using graph cuts in the kernel induced space to achieve image segmentation boils down to pinpointing the labelling that minimizes

$$F_k(\{\mu_l\}, \lambda) = \sum_{l=L} \sum_{p \in R_l} \left(\phi(\mu_l) - \phi(I_p) \right)^2 + \alpha \sum_{\{p,q\} \in N} r(\lambda(p), \lambda(q)) \tag{10}$$

where, F_k measures non Euclidean distances in the kernel induced space between the regions parameters μ_l for $1 \leq 1 \leq N$ and the observations.

At this point, we can use a very prominent machine learning method called the *kernel trick*. It involves mapping the original non-linear data from lower dimensional space into a higher dimensional space via a computationally inexpensive linear classifier. *Mercer's theorem* [38], declares that any symmetric, positive semidefinite, continuous kernel function can be put across by a scalar product in a high-dimensional space and vitally no knowledge on the explicit mapping of ϕ is required. Instead, we end up employing a kernel function, $K(y,z)$, proving

$$K(y,z) = \phi(I_p)^T . \phi(z), \quad \forall (y,z) \in X^2 \tag{11}$$

where, "." is the scalar product in the mapping/feature space. Substituting the kernel function, we get,

$$\begin{aligned} J_k(I_p, \mu) &= \left\| \phi(I_p) - \phi(\mu) \right\|^2 \\ &= (\phi(I_p) - \phi(\mu))^T . (\phi(I_p) - \phi(\mu)) \\ &= \phi(I_p)^T \phi(I_p) - \phi(\mu)^T \phi(I_p) \\ &\quad - \phi(I_p)^T \phi(\mu) + \phi(\mu)^T \phi(\mu) \\ &= K(I_p, I_p) + K(\mu, \mu) - 2K(I_p, \mu) \quad \mu \in \{\mu_l\}_{1 \leq 1 \leq N} \end{aligned} \tag{12}$$

which is the non-Euclidean distance between the original data space and its squared norm in the mapping/feature space. Simplifying Eq.(12) we obtain the following equation which represents the kernel induced segmentation functional F_k

$$\begin{aligned} F_K(\{\mu_l\}, \lambda) &= \sum_{l \in L} \sum_{p \in R_l} J_K(I_p, \mu_l) \\ &\quad + \alpha \sum_{\{p,q\} \in N} r(\lambda(p), \lambda(q)) \end{aligned} \tag{13}$$

The functional Eq.(13) depends both upon labelling $\lambda(.)$ and the regions parameters, $\{\mu_l\}_{l = 1,\ldots N}$. In the ensuing subsection, the segmentation functional optimization strategy is discussed.

5.2 OPTIMIZATION

The minimization of the functional Eq.(13) is accomplished by a two-step optimization strategy and employing a general kernel function

- The initial step involves resolving the labelling (or the wound image segment) and optimizing F_k with regard to

the statistical regions parameters $\{\mu_l\}_{l=1,\ldots N}$ by way of the *fixed point* calculation.

- The next and final step comprises of attaining the optimal partition/segment/labelling of the wound image, using the regions parameters from the initial step, by means of iterated graph cuts.

These two steps are repeated until convergence. After each step F_k is reduced with regard to a parameter. Therefore, it is a certainty that the algorithm will converge to a local minimum at the very least.

Step 1: Updating the Region Parameters:

Considering a segment of the data in image domain, the derivative of F_k with regard to μ_k, $k \in L$ the following equations are derived

$$\begin{aligned}\frac{\partial F_K}{\partial \mu_K} &= \sum_{p\in R_k}\frac{\partial J_K(I_p,\mu_k)}{\partial \mu_k}+\alpha\sum_{\{p,q\}\in N}\frac{\partial r(\lambda(p),\lambda(q))}{\partial \mu_k}\\ &= \sum_{p\in R_k}\frac{\partial}{\partial \mu_k}\left[K(\mu_k,\mu_k)-2K(I_p,\mu_k)\right]\\ &+\alpha\sum_{\substack{\{p,q\}\in N,\lambda(p)=k\\ |\mu_{\lambda(p)}-\mu_{\lambda(q)}|<const}}\left(\mu_{\lambda(p)}-\mu_{\lambda(q)}\right)\end{aligned} \quad (14)$$

Per pixel p, in the p-neighbourhood approach we choose, N_p is of size 4, i.e. the 4 × 4 pixels that surround the pixel p. Let $\overline{N}_p$ represent the set of neighbouring pixels q of p confirming $\lambda(p) \neq \lambda(q)$ and $|\mu_{\lambda(p)} - \mu_{\lambda(q)}| < const$, then Eq.(14) can be expressed as,

$$\begin{aligned}\frac{\partial F_K}{\partial \mu_K} &= \sum_{p\in R_k}\frac{\partial}{\partial \mu_k}\left[K(\mu_k,\mu_k)-2K(I_p,\mu_k)\right]\\ &+\alpha\underbrace{\sum_{p\in R_k}\sum_{q\in\overline{N}_p}\left(\mu_k-\mu_{\lambda(q)}\right)}_{\text{Sum A Sum B}},\quad k\in L\end{aligned} \quad (15)$$

The Sum A in Eq.(15) can be constrained to pixels resting on the border C_k of each partition (or region) R_k. Now, for a pixel p within the region R_k i.e. $p \in R_k$ and $p \notin C_k$, all of the neighbours q belong to R_k and hence $\overline{N}_p = \varnothing$. Taking all the above alterations into consideration Eq.(15) can be further simplified to

$$\begin{aligned}\frac{\partial F_K}{\partial \mu_K} &= \sum_{p\in R_k}\frac{\partial}{\partial \mu_k}\left[K(\mu_k,\mu_k)-2K(I_p,\mu_k)\right]\\ &+\alpha\sum_{p\in R_k}\sum_{q\in\overline{N}_p}\left(\mu_k-\mu_{\lambda(q)}\right),\quad k\in L\end{aligned} \quad (16)$$

Table.1. Prevalently Used Kernel Functions

RBF Kernel	$K(y,z)=\exp\left(-\|y-z\|^2/\sigma^2\right)$
Sigmoid Kernel	$K(y,z)=\tanh\left(c(yz)+\theta\right)$
Polynomial Kernel	$K(y,z)=(yz+c)^d$

Table.1 lists out the prevalently used kernel functions [39]. In the tests carried out in our research we made use of the Radial Basis Function (RBF) kernel as the studies in [39], [40], [41] provided us with evidence that RBF would precisely and efficiently segment the wound images. Using this kernel, the required condition to obtain a minimum of the segmentation functional F_K with regard to region parameter μ_k, $k \in L$, is the fixed point equation below,

$$\mu_k - f_{R_k}(\mu_k) = 0, \quad k \in L \quad (17)$$

where,

$$f_{R_k}(\mu_k) = \frac{\sum_{p\in R_k} I_p K(I_p,\mu_k)+\alpha\sum_{p\in C_k}\sum_{q\in\overline{N}_p}\mu_{\lambda(q)}}{\sum_{p\in R_k}K(I_p,\mu_k)+\alpha\sum_{p\in C_k}\#\overline{N}_p},\ k\in L \quad (18)$$

and the cardinality is denoted by #. By using fixed-point iterations Eq.(17) the minimum of F_K with regard to the region parameters can be calculated, the other method of calculation is using the gradient descent. This method of using the RBF kernel does not lower in complexity to that of the Gaussian model methods, as they did in the studies [31], [36]. The dissimilarity can be plainly seen in Eq.(17) i.e. updating the region parameters via fixed point computations. This calculation can simply be put as, the updating of the mean within each region when the Gaussian model is employed.

Step 2: Updating the Partitions with Graph Cut Optimization:

This step is centred on graph cut optimization and searches for the labelling that minimizes the functional F_K with respect to the partition of the image domain. The region index is represented by the term label. Let the weighted graph be given by $G = \langle V, E \rangle$, where E denotes the set of edges and V denotes the set of vertices (nodes). V not only reserves a node for each pixel but, also reserves two supplementary nodes called terminals. Generally, designated as the sink and the source. Every two separate nodes p and q have an edge $e_{\{p,q\}}$ between them. Therefore, $C \subset E$ (a graph cut) is a set of edges substantiating the following:

- In the graph $G(C) = \langle V, E \setminus C \rangle$ the terminals are separated.
- The terminals in $G(C)$ are not separated by any subset of C

When the above statements are broken down they imply that a cut denotes a group of edges, which on elimination split up the terminals and generate two subgraphs. It should also be pointed out that this cut is minimal since all of the subsets produced by it are distinct i.e. none of its subsets generate two identical subgraphs when the terminals are separated. To put it simply finding a cut C of lowest cost, in a particular graph is the minimum cut problem. The total sum of a cut's edge weights is the cost and is indicated by $|C|$. From combinatorial optimization studies of [33], we get swap moves that can be exercised to find a local minimum of functional F_K by efficiently calculating the minimum cost cuts, once the weights of graph G are set appropriately. Swap moves are carried out per pair of labels $\{\theta,\beta\}$, in order to pinpoint the minimum cut in the subgraph $G_{\theta,\beta} = \langle V_{\theta,\beta}, E_{\theta,\beta} \rangle$. $P_{\theta,\beta} \cup \{\theta,\beta\}$ is identical to the set $V_{\theta,\beta}$ i.e. it comprises of the set $(P_{\theta,\beta})$ of terminals θ and β and vertices (or nodes) labelled θ or β. The set $E_{\theta,\beta}$ comprises of the edges that both connect the terminals θ and β to the nodes of $P_{\theta,\beta}$ as well as connect the nodes of $P_{\theta,\beta}$ to each other.

Table.2. The Weights Assigned To The Graph Edges

Edge	Weight	For
$\{P_{\theta,\beta}\}$	$J_K(I_p,\theta)+\sum_{\substack{\{p,q\}\in N_p \\ q\notin P_{\theta,\beta}}} r(\theta,\lambda(q))$	$p \in P_{\theta,\beta}$
$\{P_{\theta,\beta}\}$	$J_K(I_p,\theta)+\sum_{\substack{\{p,q\}\in N_p \\ q\notin P_{\theta,\beta}}} r(\beta,\lambda(q))$	$p \in P_{\theta,\beta}$
$e_{\{p,q\}}$	$r(\theta,\beta)$	$\{p,q\}\in N$ $p,q \in P_{\theta,\beta}$

Obtaining the region parameters from the first step, this step involves reiterating the search for the minimum cut over every pair of labels on the sub graph $P_{\theta,\beta}$ until it an optimal solution is found. In order to find the optimal minimum cut, the weights must to be set *dynamically* every time the pair of labels and/or the region parameters change. Table.2 shows the different kinds of weights allocated to the graph edges so that the functional given by Eq.(13) can be minimized with regard to a specific partition.

6. EXPERIMENTAL RESULTS

In this section the results of the two methods are shown. The results shown below are obtained from a large dataset of images. We also demonstrate the flexibility and efficacy of the two methods when used for a variety of wound images. It should also be noted that all the images used here are real. All the images used in our experiments are of different shapes and sizes and contain all the different types of tissues explained in the introduction. The images were obtained from hospitals and from online databases such as the Medetec image *databases*.

6.1 USING THE GABOR FILTER BANK TO SEGMENT THE IMAGE

As already explained in section 2, Gabor Filters are used in the first method to segment the image. The results confirm that the Gabor Filter method of unsupervised image segmentation can be used to obtain relatively accurate results in a feasible amount of time. As we see in Fig.5, the Gabor Filter method is able to detect all three kinds of tissues namely Granulation, Slough and Necrosis. Since, the colours are to represent each region are chosen at runtime the different tissues are arbitrary. The segmentation is performed solely on the texture data and hence this method is computationally attractive and for the short period this method takes to provide the user with an output it is very accurate.

The images are first smoothed using a Gaussian Filter. This is done in order to eradicate any noise present in the image. Once this is done the Gabor Filter Bank is generated and the input image is filtered iteratively using the Gabor Filter Bank. By doing so, we obtain several multi-channel filtered images. Finally we obtain a segmented image by reconstructing the input image from the set of filtered images. The images labelled (a) – (e) are the input images and the images labelled (f) – (j) are the segmented images.

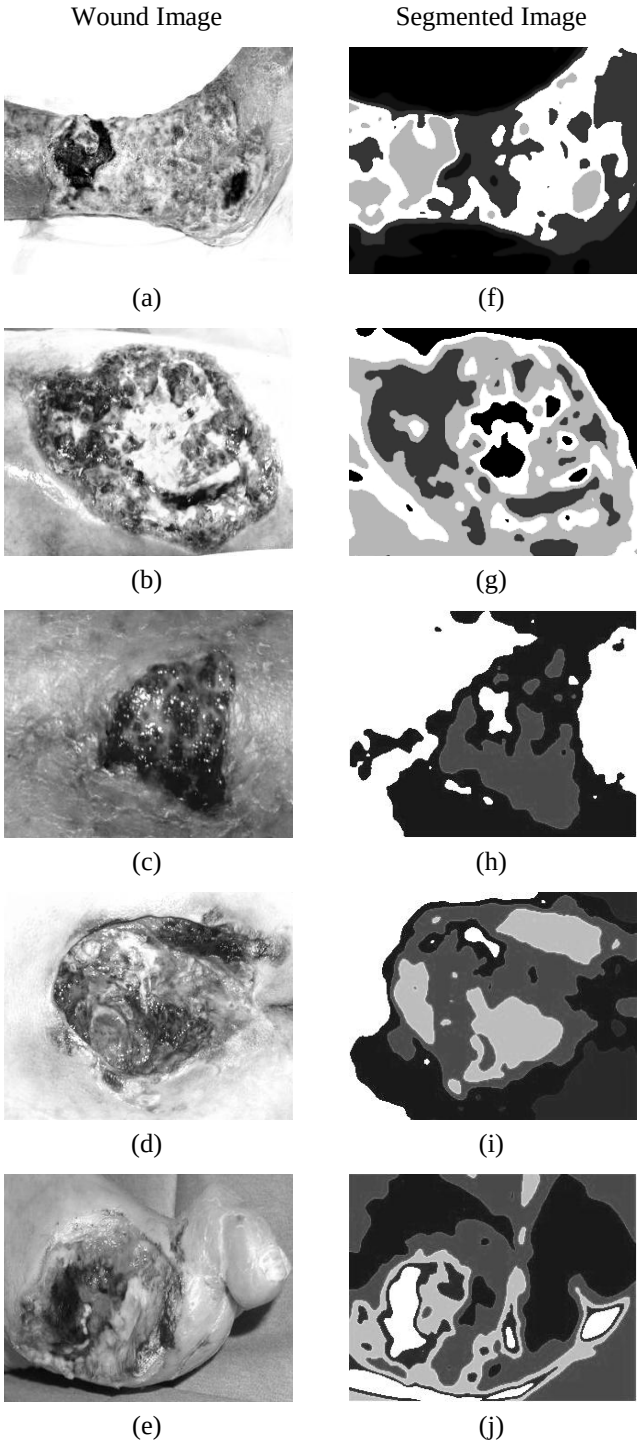

Fig.5. The Gabor Filtered and segmented images

6.2 USING PARAMETRIC KERNEL GRAPH CUTS TO SEGMENT THE IMAGE

The results from the Gabor Filtered images are not completely accurate. So, we invested our time in another method to see if were able to obtain better results. From prior background studies, Graph Cuts were proven to segment images with good accuracy in an unsupervised manner. The results of

the wound image segmentation furnished below are acquired using an enhanced version of the optimized graph cut method that is, the Parametric Kernel Graph Cuts [28]. Using this method the segmentation obtained was much more precise. In most cases the results were near perfect as seen in Fig.6. When using this method it was seen that even the depth of the wounds could be distinguished from two dimensional images. As illustrated in the Fig.6, the boundaries of the wounds are precisely located and thus, the various tissues are identified. Since the graph cut method labels the uniform regions with similar weights the various partitions are labelled in the same manner even if they are disconnected. It should also be noted that the segmentation produced by unsupervised parametric kernel graph cuts is very consistent in its working, as the results after do not change with each run.

The images labelled (a) – (e) are the input wound images, the images labelled (f) – (j) are the partitioned images and the images labelled (k) – (o) are the segmented images. The partitioned images here show how the regions have been assigned for segmentation.

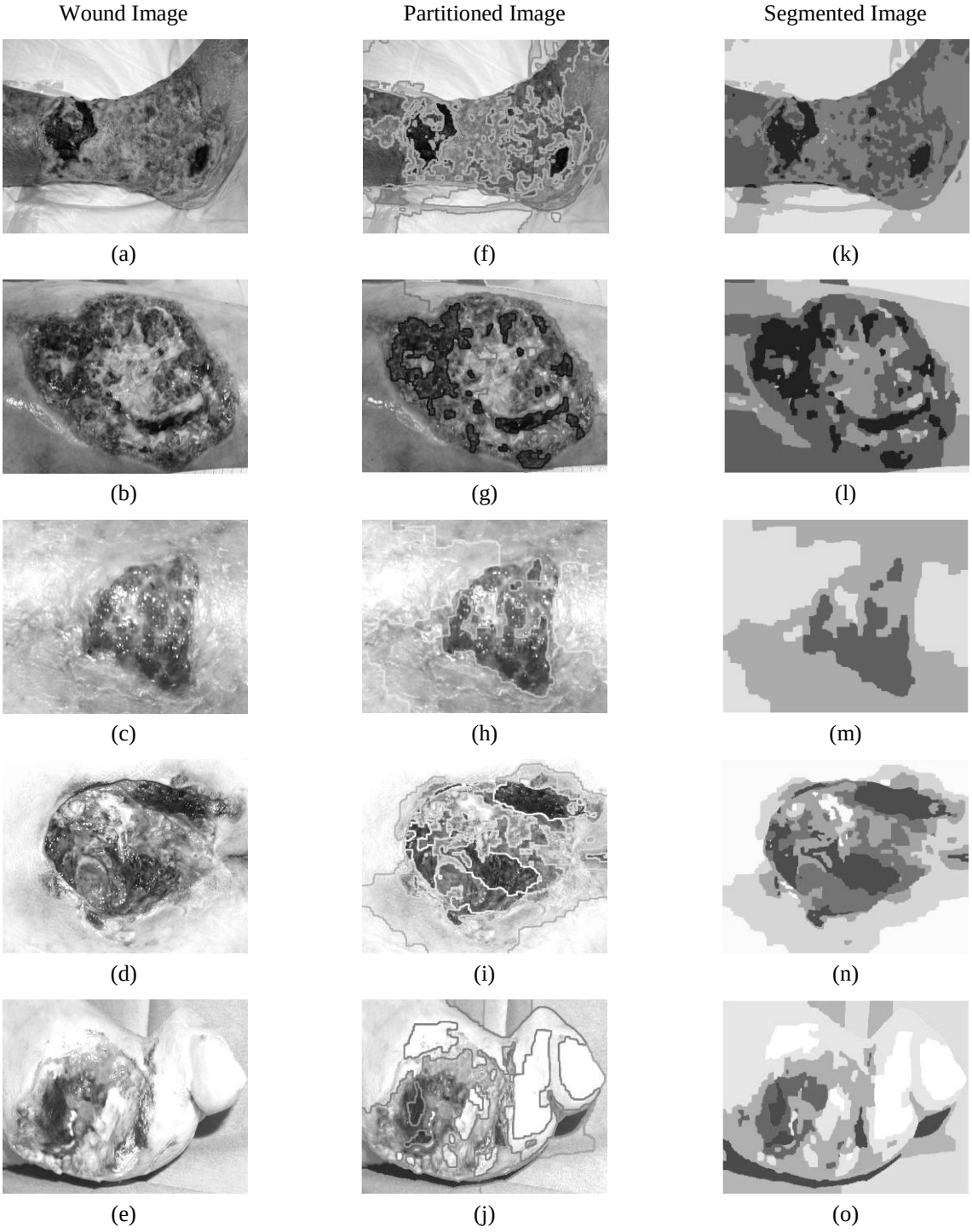

Fig.6. Segmented using Parametric Kernel Graph Cuts

7. CONCLUSION AND FUTURE SCOPE

This study investigated two methods for wound image segmentation. The first one was by using Gabor Filters. This method is implemented by segmenting the wound image using its various textures. The segmentation is carried out using a large number of two dimensional Gabor Filters called a Gabor Filter Bank to filter the wound image. Feature extraction, clustering and finally segmentation of the wound image. The second method involved using the multiregion graph cut in a kernel-induced space. In the second method a variety of features such as colour, intensity, pixel relationships, texture vectors and spatial location of pixels was used for the segmentation of the wound image. This method involved minimization of a functional obtained via transforming image data by means of a kernel function. The optimization algorithm ensures that both efficiency and accuracy are conserved. A large number of experiments on real wound images showed the efficacy and flexibility of these methods.

In order to improve upon the methods discussed in our research we suggest that for the first method one can use the concept of training the system to obtain a reduced set of filters comprising the Gabor Filter Bank. In our case the implementation of the second method the RBF kernel was used. The RBF kernel was used to reduce both complexity and computation time. In cases where, they're not considered constraints i.e. an unconstrained optimization problem, different kernels and a combination of kernels can be used. The development of a 3D wound image can be used to judge the depth of the wound accurately. This involves using images that were captured during the same time having a similar lighting arrangement, as the shadows present in the image play a vital role in the discrimination of the depth of the wound.

REFERENCES

[1] V. Falanga, "Wound healing and its impairment in the diabetic foot", *Lancet*, Vol. 366, No. 9498, pp. 1736–1743, 2005.

[2] M. D. Kerstein, "The scientific basis of healing", *Advances in Wound Care*, Vol. 10, No. 3, pp. 30 – 36, 1997.

[3] D. P. Kane, "*Chronic wound healing and chronic wound management*", In: Krasner D. L, Rodeheaver G. T, Sibbald R. G. eds: Chronic Wound Care: A Clinical Source Book for Healthcare Professionals, 4th Edition, Health Management Publications, pp. 7-17, 2001.

[4] B. Coulomb, P. Saiag, E. Bell, F. Breitburd, C. Lebreton, M. Heslan, and L. Dubertret, "A new method for studying epidermalization in vitro", *British Journal of Dermatology*, Vol. 114, No. 1, pp. 91 – 101, 1986.

[5] Sir Stanley Davidson and John MacLeod, "*Davidson's Principles and Practice of Medicine: a textbook for students and doctors*", 13th Edition, Churchill Livingstone, pp. 590 - 592, 1981.

[6] Hazem Wannous, Yves Lucas and Sylvie Treuillet, "Efficient SVM classifier based on color and texture region features for wound tissue images", *Proceedings of SPIE, Medical Imaging: Computer-Aided Diagnosis*, Vol. 6915, 2008.

[7] J. R. Mekkes and W. Westerhof, "Image processing in the study of wound healing", *Clinical Dermatology*, Vol. 13, No. 4, pp. 401 – 407, 1995.

[8] Thomas A. Krouskop, Robert Baker and Michael S. Wilson, "A noncontact wound measurement system", *Journal of Rehabilitation Research and Development*, Vol. 39, No. 3, pp. 337 – 346, 2002.

[9] William Paul Berriss and Stephen John Sangwine, "Automatic Quantitative Analysis of Healing Skin Wounds using Colour Digital Image Processing", *World Wide Wounds*, Vol. 1, No. 1, 1997.

[10] M. Herbin, F. X. Bon, A. Venot, F. Jenlouis and M. L. Dubertret, "Assessment of healing kinetics through true color image processing", *IEEE Transactions on Medical Imaging*, Vol. 12, No. 1, pp. 39 – 43, 1993.

[11] Thomas Gilman, "Wound outcomes: The utility of surface measures", *International Journal of Lower Extremity Wounds*, Vol. 3, No. 3, pp. 125 – 132, 2004.

[12] P. Plassmann, K. G. Harding and J. M. Melhuish, "Methods of Measuring Wound size - A Comparative Study", *Wounds*, Vol. 6, No. 2, pp. 54 – 61, 1994.

[13] David H. Keast, C. Keith Bowering, A. Wayne Evans, Gerald L. Mackean, Catherine Burrows and Lincoln D'Souza, "MEASURE: A proposed assessment framework for developing best practice recommendations for wound assessment", *Wound Repair and Regeneration*, Vol. 12, No. 3, pp. S1 – S17, 2004.

[14] Mark E. Roberts and Ela Claridge, "An artificially evolved vision system for segmenting skin lesion images", *Proceedings of the 6th International Conference on Medical Image Computing and Computer-Assisted Intervention*, Vol. 2878, pp. 655 – 662, 2003.

[15] Julien Mairal, Michael Elad and Guillermo Sapiro, "Sparse Representation for Color Image Restoration", *IEEE Transactions on Image Processing*, Vol. 17, No. 1, pp. 53 – 69, 2008.

[16] Sylvie Treuillet, Benjamin Albouy and Yves Lucas "Three-Dimensional Assessment of Skin Wounds Using a Standard Digital Camera", *IEEE Transactions on Medical Imaging*, Vol. 28, No. 5, pp. 752 – 762, 2009.

[17] Hazem Wannous, Yves Lucas and Sylvie Treuillet, "Enhanced Assessment of the Wound- Healing Process by Accurate Multiview Tissue Classification", *IEEE Transactions on Medical Imaging*, Vol. 30, No. 2, pp. 315–326, 2011.

[18] Perona and Malik, "Preattentive texture discrimination with early vision mechanisms", *Journal of Optical Society of America*, Vol. 7, No. 5, pp. 923 – 932, 1990.

[19] D. Clausi and M. Ed Jernigan, "Designing Gabor filters for optimal texture separability", *Pattern Recognition*, Vol. 33, pp. 1835 – 1849, 2000.

[20] Jianguo Zhang, Tieniu Tan and Li Ma, "Invariant texture segmentation via circular gabor filter", *Proceedings of the 16th IAPR International Conference on Pattern Recognition*, Vol. II, pp. 901 – 904, 2002.

[21] K. Jain and F. Farrokhnia, "Unsupervised texture segmentation using Gabor filters", *Pattern Recognition*, Vol. 24, No. 12, pp. 1167 – 1186, 1991.

[22] John G. Daugman: "Uncertainty relations for resolution in space, spatial frequency, and orientation optimized by two-

dimensional visual cortical filters", *Journal of the Optical Society of America A*, Vol. 2, No. 7, pp. 1160 – 1169, 1985.

[23] F. W. Campbell and J. G. Robson, "Application of Fourier Analysis to the Visibility of Gratings", *Journal of Physiology*, Vol. 197, No. 3, pp. 551 – 566, 1968

[24] R. Nock and F. Nielsen, "Statistical Region Merging", *IEEE Transactions on Pattern Analysis and Machine Intelligence*, Vol. 26, No. 11, pp. 1452 – 1458, 2004.

[25] Y. G. Wang, J. Yang and Y. C. Chang "Color-texture image segmentation by integrating directional operators into JSEG method", *Pattern Recognition Letters*, Vol. 27, No. 16, pp. 1983 – 1990, 2006.

[26] Patrik Sturm and Lutz Priese, "3D-Color-Structure-Code: A hierarchical region growing method for segmentation of 3D-images", *Proceedings of the 13th Scandinavian Conference on Image Analysis*, pp. 603-608, 2003.

[27] Y. Boykov, O. Veksler and R. Zabih, "Fast approximate energy minimization via graph cuts", *IEEE Transactions on Pattern Analysis and Machine Intelligence*, Vol. 23, No. 11, pp. 1222 – 1239, 2001.

[28] M. B. Salah, A. Mitiche and I. B. Ayed, "Multiregion Image Segmentation by Parametric Kernel Graph Cuts" *IEEE Transactions on Image Processing*, Vol. 20, No. 2, pp. 545 – 557, 2011.

[29] Y. Boykov and M.-P. Jolly, "Interactive graph cuts for optimal boundary and region segmentation of objects in N-D images", *Proceedings of IEEE International Conference on Computer Vision*, Vol. I, pp. 105 – 112, 2001.

[30] Y. Boykov and G. Funka-Lea, "Graph cuts and efficient N-D image segmentation," *International Journal on Computer Vision*, Vol. 70, No. 2, pp. 109 – 131, 2006.

[31] Blake, C. Rother, M. Brown, P. Perez and P. Torr, "Interactive image segmentation using an adaptive GMMRF model", *Proceedings of European Conference on Computer Vision*, Vol. 1, pp. 428 – 441, 2004.

[32] Rother, V. Kolmogorovy and A. Blake, "Grabcut-interactive foreground extraction using iterated graph cuts", *ACM Transactions on Graphics*, Vol. 23, No. 3, pp. 309–314, 2004.

[33] B. Ayed, A. Mitiche and Z. Belhadj, "Multiregion level-set partitioning of synthetic aperture radar images", *IEEE Transactions on Pattern Analysis on Machine Intelligence*, Vol. 27, No. 5, pp. 793–800, 2005.

[34] R. Zabih and O. Veksler, "Efficient graph-based energy minimization methods in computer vision", Ph.D dissertation, Cornell University, Ithaca, NY, 1999.

[35] N. Vu and B. S. Manjunath, "Shape prior segmentation of multiple objects with graph cuts", *Proceedings of IEEE International Conference on Computer Vision and Pattern Recognition*, pp. 1–8, 2008.

[36] M. B. Salah, A. Mitiche and I. B. Ayed, "A continuous labeling for multiphase graph cut image partitioning", *Proceedings of the 4th International Symposium on Advances in Visual Computing*, pp. 268–277, 2008.

[37] N. Y. El-Zehiry and A. Elmaghraby, "A graph cut based active contour for multiphase image segmentation", *Proceedings of 15th IEEE International Conference on Image Processing*, pp. 3188–3191, 2008.

[38] K. R. Muller, S. Mika, G. Ratsch, K. Tsuda and B. Scholkopf, "An introduction to kernel-based learning algorithms", *IEEE Transactions on Neural Networks*, Vol. 12, No. 2, pp. 181–201, 2001.

[39] S. Dhillon, Y. Guan, and B. Kulis, "Weighted graph cuts without eigenvectors: A multilevel approach," *IEEE Transactions on Pattern Analysis and Machine Intelligence*, Vol. 29, No. 11, pp. 1944–1957, 2007.

[40] D. Zhang and S Chen, "Fuzzy clustering using kernel methods", *Proceedings of the International Conference on Control Automation*, pp. 123–127, 2002.

[41] P. J. Huber, "*Robust Statistics*", Wiley-Interscience, 1981.

[42] P. Kohli, J. Rihan, M. Bray and P. H. S. Torr, "Simultaneous segmentation and pose estimation of humans using dynamic graph cuts", *International Journal of Computer Vision*, Vol. 79, No. 3, pp. 285–298, 2008.

[43] V. Kolmogorov, A. Criminisi, A. Blake, G. Cross and C. Rother, "Probabilistic fusion of stereo with color and contrast for bilayer segmentation", *IEEE Transactions on Pattern Analysis and Machine Intelligence*, Vol. 28, No. 9, pp. 1480–1492, 2006.

[44] X. Liu, O. Veksler and J. Samarabandu, "Graph cut with ordering constraints on labels and its applications", *Proceedings of the IEEE International Conference Computer Vision and Pattern Recognition*, pp. 1–8, 2008.

[45] V. Kolmogorov and R. Zabih, "What Energy Functions Can Be Minimized via Graph Cuts?", *IEEE Transactions on Pattern Analysis and Machine Intelligence*, Vol. 26, No. 2, pp. 147-159, 2004.

[46] Y. Boykov and V. Kolmogorov, "An Experimental Comparison of Min-Cut/Max-Flow Algorithms for Energy Minimization in Vision", *IEEE Transactions on Pattern Analysis and Machine Intelligence*, Vol. 26, No. 9, pp. 1124-1137, 2004.

[47] M. Mignotte, C. Collet, P. Pérez, and P. Bouthemy, "Sonar image segmentation using an unsupervised hierarchical MRF model", *IEEE Transactions on Image Processing*, Vol. 9, No. 7, pp. 1216–1231, 2000.

[48] S. C. Zhu, "Statistical modelling and conceptualization of visual patterns", *IEEE Transactions on Pattern Analysis and Machine Intelligence*, Vol. 25, No. 6, pp. 691–712, 2003.

[49] Jain, P. Duin and J. Mao, "Statistical pattern recognition: A review", *IEEE Transactions on Pattern Analysis and Machine Intelligence*, Vol. 22, No. 1, pp. 4–37, 2000.

[50] B. Scholkopf, A. Smola and K. R. Muller, "Nonlinear component analysis as a kernel eigenvalue problem", *Neural Computation*, Vol. 10, No. 5, pp. 1299–1319, 1998.

[51] T. M. Cover, "Geomeasureal and statistical properties of systems of linear inequalities in pattern recognition", *IEEE Transactions on Electronic Computers*, Vol. EC-14, pp. 326–334, 1965.

[52] M. Girolami, "Mercer kernel based clustering in feature space", *IEEE Transactions on Neural Networks*, Vol. 13, No. 3, pp. 780–784, 2001.

[53] C. Vazquez, A. Mitiche and I. B. Ayed, "Image segmentation as regularized clustering: A fully global curve evolution method", *Proceedings of the International Conference on Image Processing*, Vol. 5, pp. 3467–3470, 2004.